CHAPTER 6

DYNAMIC MECHANICAL ANALYSIS OF NBR/EVA BLENDS

The results of this chapter have been communicated to *Polymer*

Dynamic mechanical test methods have been widely employed for investigating the structure-property relations and viscoelastic behaviour of polymeric materials.[1,2] The dynamic properties of polymeric materials are of considerable practical significance for several reasons, particularly if they are determined over wide range of frequencies and temperatures. They can provide insight into various aspects of material structure besides being a convenient measure of polymer transition temperatures. The dynamic properties are also of direct relevance to a range of unique polymer applications, concerned with the isolation of vibrations or dissipation of vibrational energy in engineering components.[2]

The effect of microstructure on the viscoelasticity of polycarbonate/styrene-acrylonitrile copolymer (PC/SAN) blend has been studied by Guest *et al.*[3] The reactive compatibilisation of PVC/ENR blends using carboxylated nitrile rubber (XNBR) in terms of dynamic mechanical analysis (DMA) was reported by Ramesh and De.[4] They found that an immiscible composition of PVC/ENR blend becomes progressively miscible by the addition of XNBR. Varughese *et al.*[5] studied the miscibility of PVC with 50% epoxidised natural rubber (ENR) using DMA. A single T_g between the T_gs of the pure components revealed the miscibility of the system. Sequential interpenetrating polymer networks (IPN) based on nitrile rubber (NBR) and poly(vinyl acetate) (PVAc) have been synthesised by Patri *et al.*[6] The

properties of these IPNs were investigated by tensile test, DSC, DMA and swelling measurement. IPNs having 2 and 5% crosslinker showed splitting in the tanδ peak. On increasing the crosslinker concentration to 9% and beyond, the splitting disappeared. The damping capability of the IPNs has been explained in terms of the magnitude of tan δ, area under the tan δ curve and the peak width at half height. Calorimetric and dynamic mechanical analyses demonstrate that poly(vinyl acetate) tends to compatibilise blends of poly(vinylidene fluoride)/polystyrene (PVF_2/PS).[7] The viscoelastic behaviour of binary and ternary blends of cis-1,4-polyisoprene, 1,4-polybutadiene and polyisoprene-polybutadiene block copolymer was explained in terms of the mechanical model of Takayanagi by Cohen and Ramos.[8]

Cho *et al.*[9] carried out dynamic mechanical analysis to investigate the miscibility and melting behaviour of blends of vinylidene fluoride with tetrafluoroethylene and hexafluoroacetone copolymers. Investigations on the compatibility of polycarbonate (PC) with polystyrene (PS) by Li *et al.*[10] using dynamic mechanical measurements indicated that PC/PS system is partially miscible.

The viscoelastic and thermal properties of blends of natural rubber (NR) and ethylene-vinyl acetate copolymer (EVA) were reported by Koshy *et al.*[11] The damping factor of these blends increased with increase in rubber content, and was correlated with the phase morphology of the system.

The effect of blend composition, crosslinking system and frequency on the viscoelastic response of NBR/EVA blends is discussed in this chapter. Cole-Cole analysis is carried out to investigate the extent of miscibility of the blends. A master curve for the modulus of the blend is generated by applying the time-temperature superposition principle.

6.1 Results and discussion

6.1.1 *Effect of blend composition*

The loss tangent (tan δ) values of the component copolymers and the uncrosslinked blends at 50 Hz as a function of temperature (-70 to 20°C) are shown in Figure 6.1. The glass transition temperature of NBR is at –8°C and that of EVA at –11.5°C. In the case of blends, there is a single, sharp transition which shifts slightly towards the low temperature region with blend ratio. Since the T_gs of the polymers are very close, miscibility cannot be judged from T_g measurements. Figure 6.2 presents the dependence of tan δ_{max} on the weight percentage of NBR in the blend. It is observed that the damping properties of the blends increase with increasing NBR content. The tan δ_{max} values show a gradual increase up to 50% of NBR followed by a sharp increase at a high content of NBR. This is because of the fact that there occurs a phase inversion in the morphology of the blend from N_{50} onwards as evident from the scanning electron micrographs discussed earlier (Figure 3.2).

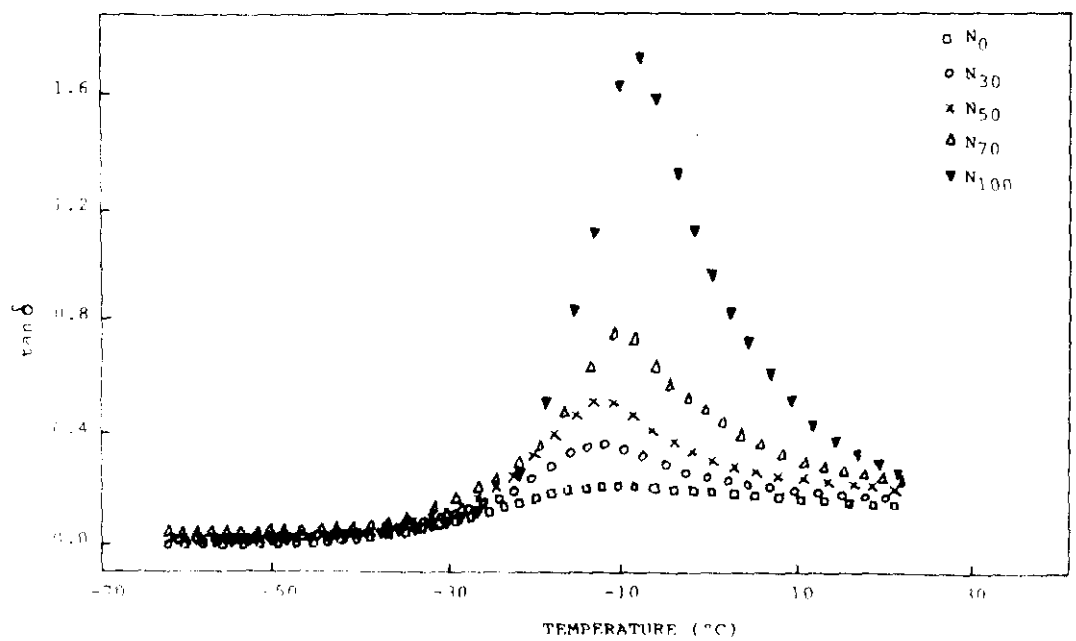

Figure 6.1. The effect of temperature on the tan δ values of uncrosslinked NBR/EVA blends

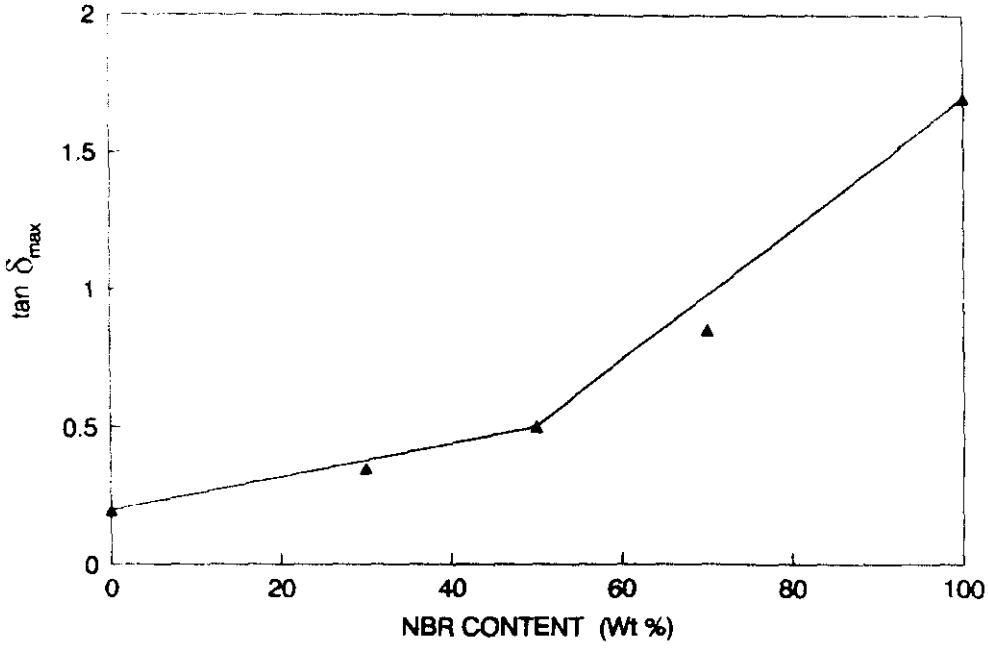

Figure 6.2. The variation of tan δ_{max} with weight percentage of NBR

The influence of temperature on the storage modulus of the blends is depicted in Figure 6.3. The curves for all the compositions have three distinct regions: a glassy region, a transition region and a rubbery region. In the glassy region all the blends exhibit nearly same moduli. In the rubbery region (above T_g) NBR rich blends exhibit lower modulus. Above T_g, NBR changes from the glassy state to amorphous state. Also, on increasing the NBR content the crystallinity is reduced. Therefore the modulus of NBR rich blends decreases at higher temperatures.

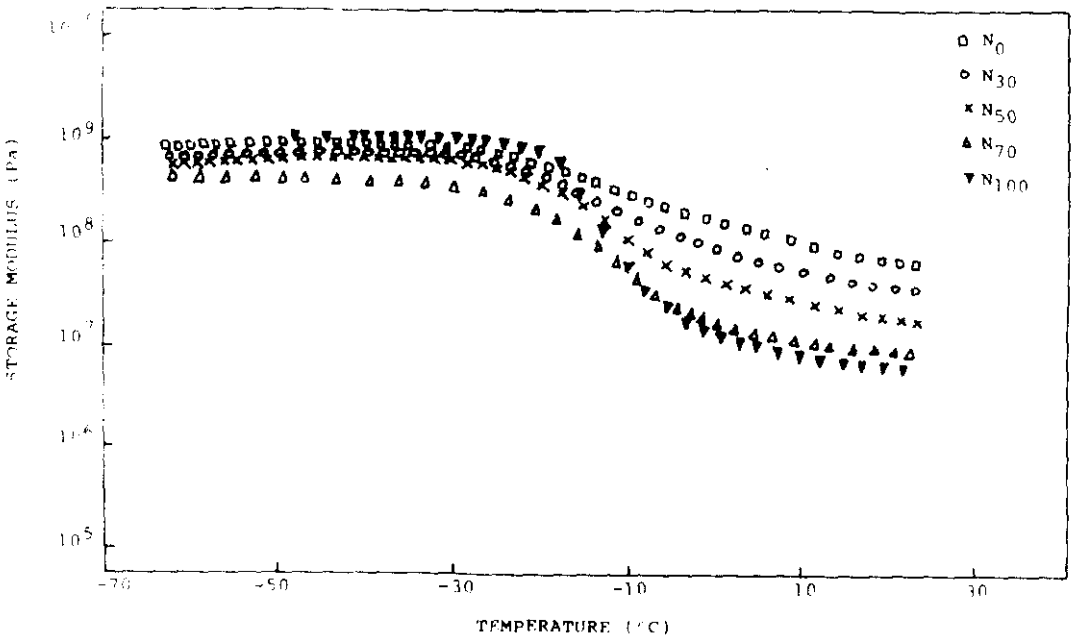

Figure 6.3. The effect of temperature on the storage modulus of uncrosslinked NBR/EVA blends

The tan δ values of the peroxide cured homopolymers and blends as a function of temperature (-70 to 20°C) at 50 Hz are shown in Figure 6.4. The glass transition temperature of peroxide cured NBR ($N_{100}P$) is -4°C and that of EVA (N_0P) is -10.4°C. The effect of blend composition on T_g and tan δ_{max} of uncrosslinked and peroxide cured NBR/EVA blends are given in Table 6.1. In both the cases, tan δ_{max} increases with an increase in NBR content, i.e., the damping properties of the blends increase with increasing nitrile rubber content. The T_g of the blends are in between that of the pure components. Uncrosslinked blends exhibit a lower T_g than that of the peroxide cured blends. This can be attributed to the restrictions in chain flexibility of crosslinked systems. The variation in tan δ at higher temperatures (20 to 120°C) are presented in Figure 6.5. For all the samples, except $N_{100}P$, a transition is observed around 80°C which is due to the melting of EVA.

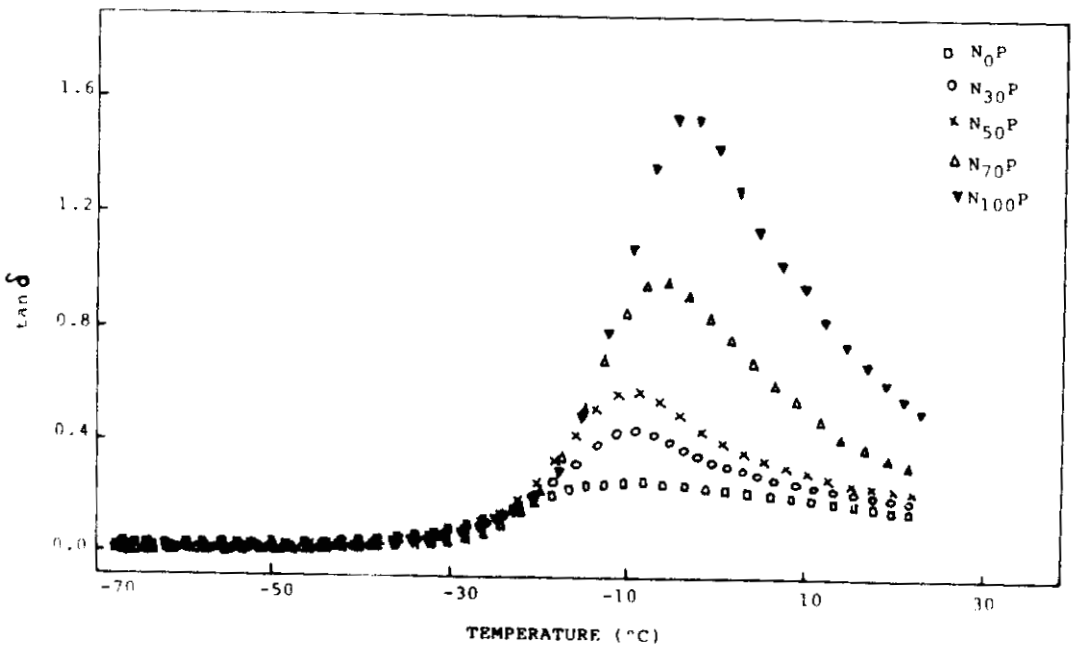

Figure 6.4. The effect of temperature (–70 to 20°C) on the tan δ values of peroxide cured NBR/EVA blends

Table 6.1. T_g and tan δ_{max} of uncrosslinked and peroxide cured NBR/EVA blends at 50 Hz

Composition	Uncrosslinked		Peroxide cured	
	tan δ_{max}	T_g (°C)	tan δ_{max}	T_g (°C)
N_0	0.19	-11.5	0.24	-10.4
N_{30}	0.34	-11.0	0.42	-9.2
N_{50}	0.49	-12.0	0.58	-9.0
N_{70}	0.77	-10.5	0.96	-6.0
N_{100}	1.75	-8.0	1.55	-4.0

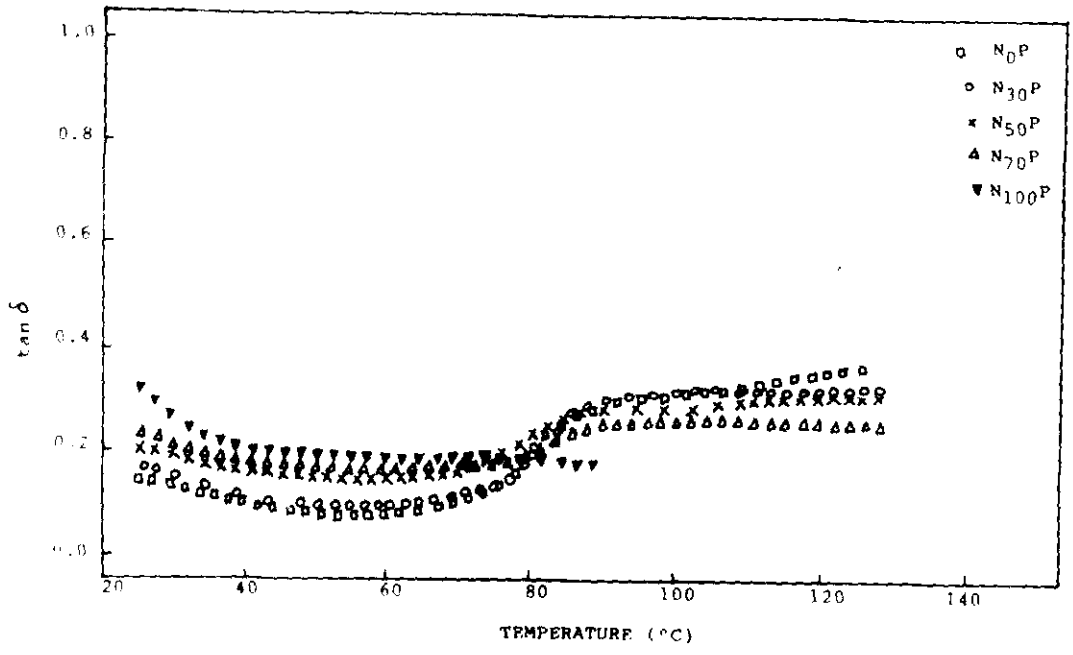

Figure 6.5. The effect of temperature (20 to 120°C) on the tan δ values of peroxide cured NBR/EVA blends

The influence of temperature (-70 to 20°C) on the storage and loss moduli of the peroxide cured blends at 50 Hz is given in Figures 6.6 and 6.7 respectively. Similar results as in the case of uncrosslinked blends are obtained, i.e., all compositions exhibit three distinct regions corresponding to the glassy, transition and rubbery regions. The E″ versus temperature curves show sharp loss peaks for the blend compositions. At higher temperatures (above T_g), the modulus decreases with the increase in NBR content. The changes in the storage and loss moduli of peroxide cured blends at higher temperatures (20–120°C) are shown in Figures 6.8 and 6.9 respectively. Up to the melting temperature of EVA, both the storage and loss moduli values decrease with the increase in NBR content. Afterwards, the trend is reversed, i.e., the blends exhibit a marginal increase in the moduli value with NBR content.

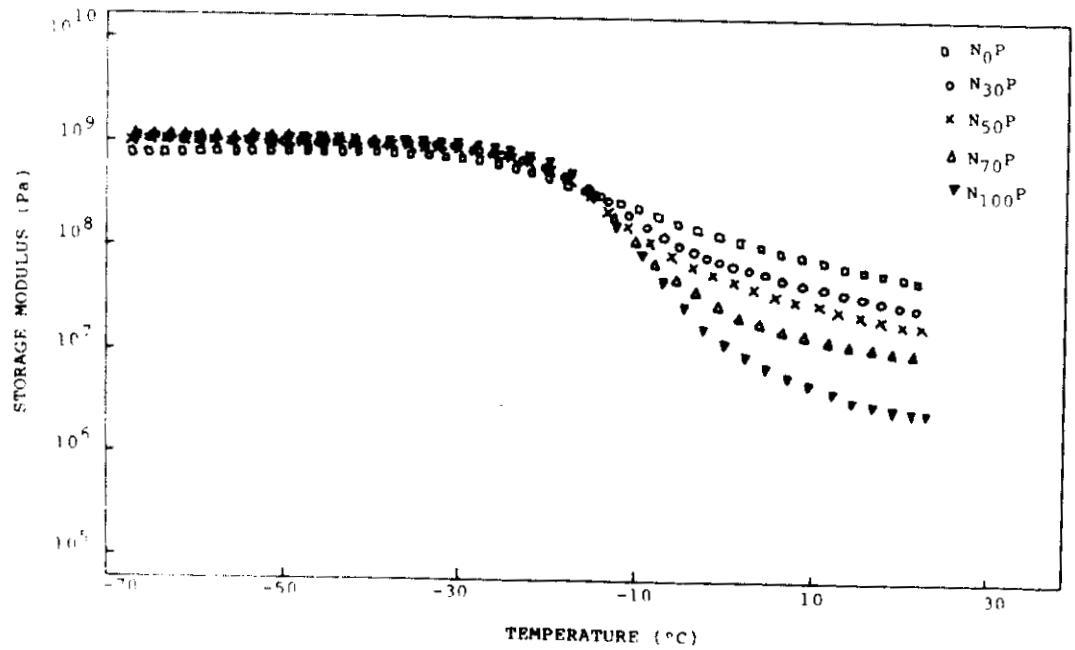

Figure 6.6. The influence of temperature (–70 to 20°C) on the storage modulus of peroxide cured NBR/EVA blends

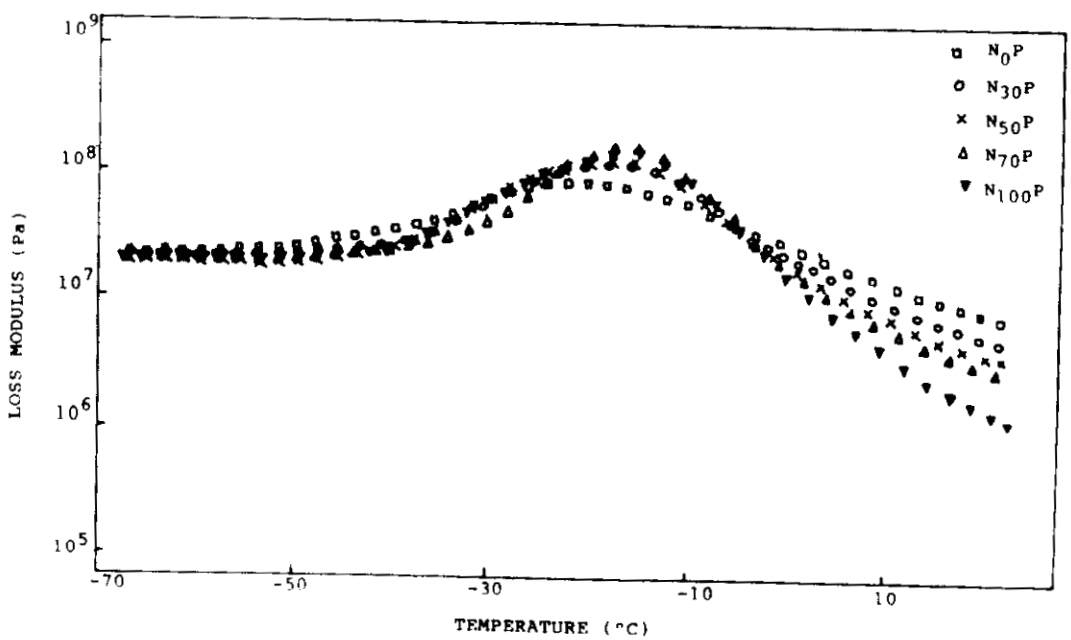

Figure 6.7. The influence of temperature (–70 to 20°C) on the loss modulus of peroxide cured NBR/EVA blends

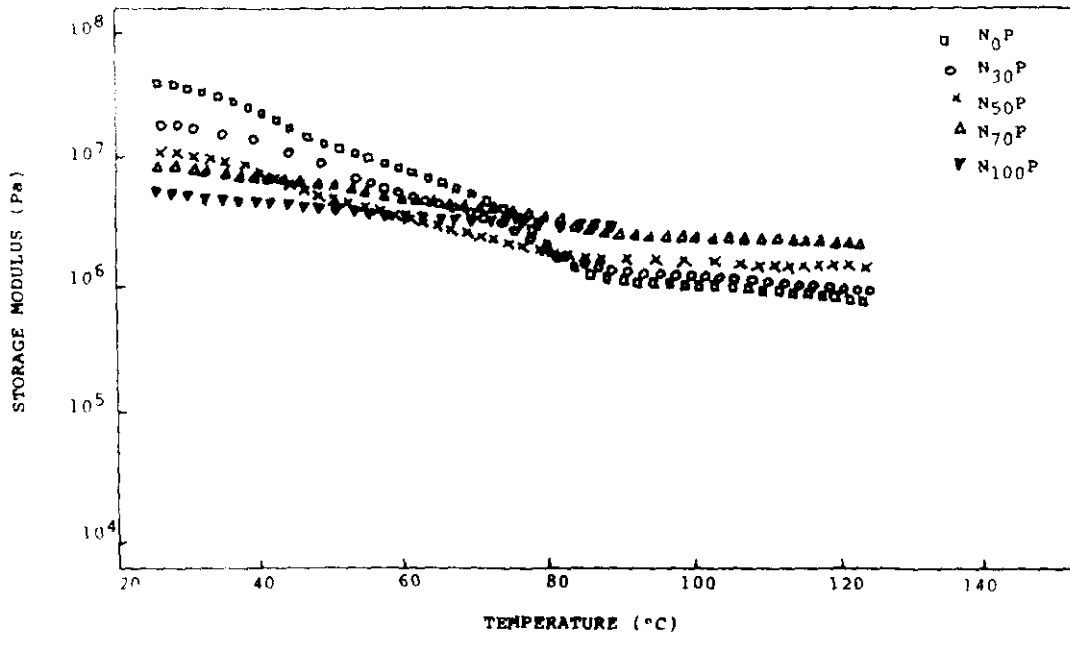

Figure 6.8. The influence of temperature (20 to 120°C) on the storage modulus of peroxide cured NBR/EVA blends

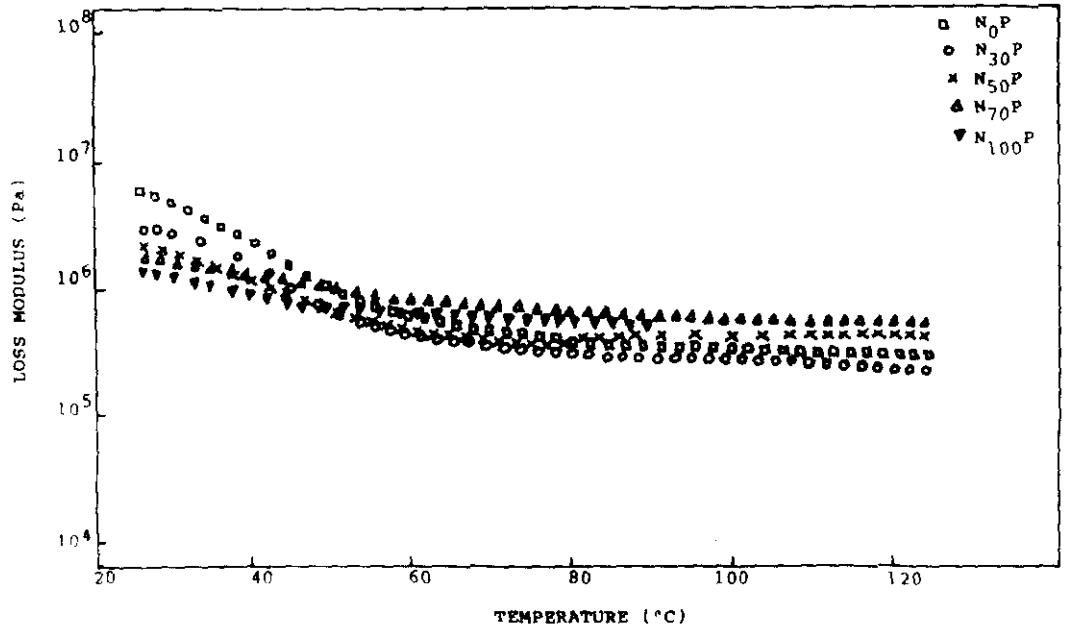

Figure 6.9. The influence of temperature (20 to 120°C) on the loss modulus of peroxide cured NBR/EVA blends

The glass transition temperature of peroxide cured NBR/EVA blends from the peaks of tan δ and E″ (loss modulus) at 50 Hz is compared in Table 6.2. As usual, in all the cases the T_g obtained from tan δ peak is greater than that obtained from E″ peak [1]

Table 6.2. Comparison of T_g of peroxide cured NBR/EVA blends based on peak values of tan δ and loss modulus (E″) at 50 Hz

Composition	T_g (°C)	
	tan δ peak	E″ peak
N_0P	-10.4	-20.0
$N_{30}P$	-9.2	-17.5
$N_{50}P$	-9.0	-17.0
$N_{70}P$	-6.0	-15.5
$N_{100}P$	-4.0	-15.0

6.1.2 Effect of frequency

The dynamic mechanical properties of peroxide cured NBR/EVA blends are analysed from -70 to 20°C at different frequencies (0.1, 1, 10, 50 and 100 Hz). The tan δ values of $N_{50}P$ at different frequencies as a function of temperature are given in Figure 6.10. The glass transition temperature is shifted towards the high temperature region with increasing frequency (Table 6.3). This is also evident from Figure 6.11 where the glass transition temperature of $N_{50}P$ is plotted against frequency. The tan δ_{max} of peroxide cured blends at different frequencies are given in Table 6.4. There is only a marginal increase in tan δ_{max} values with increasing frequency, i.e., the damping characteristics of the blends are not much affected by the variations in frequency. The tan δ values of $N_{50}P$ at three different temperatures are plotted as a function of frequency in Figure 6.12. Below the transition region

(-30°C), the tan δ values decrease with frequency. In the transition region (-10°C) and above T_g(10°C), the tan δ values increase with frequency.

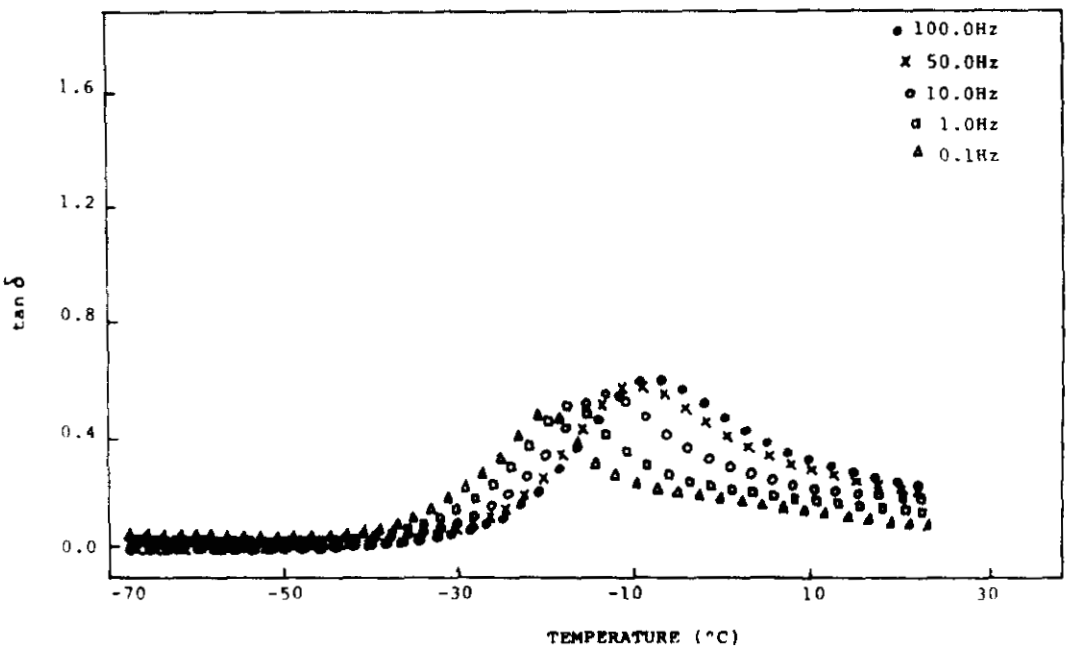

Figure 6.10. The variation in tan δ values of $N_{50}P$ at different frequencies as a function of temperature

Table 6.3. Effect of blend composition and frequency on the T_g (°C) values from tan δ peak

Frequency (Hz)	Blend composition				
	N_0P	$N_{30}P$	$N_{50}P$	$N_{70}P$	$N_{100}P$
0.1	-21.4	-19.0	-20.0	-18.2	-15.9
1.0	-18.2	-16.4	-17.0	-14.1	-12.0
10.0	-13.2	-13.4	-13.5	-10.0	-8.6
50.0	-10.4	-9.2	-9.0	-6.0	-4.0
100.0	-7.3	-7.7	-6.8	-3.4	-0.9

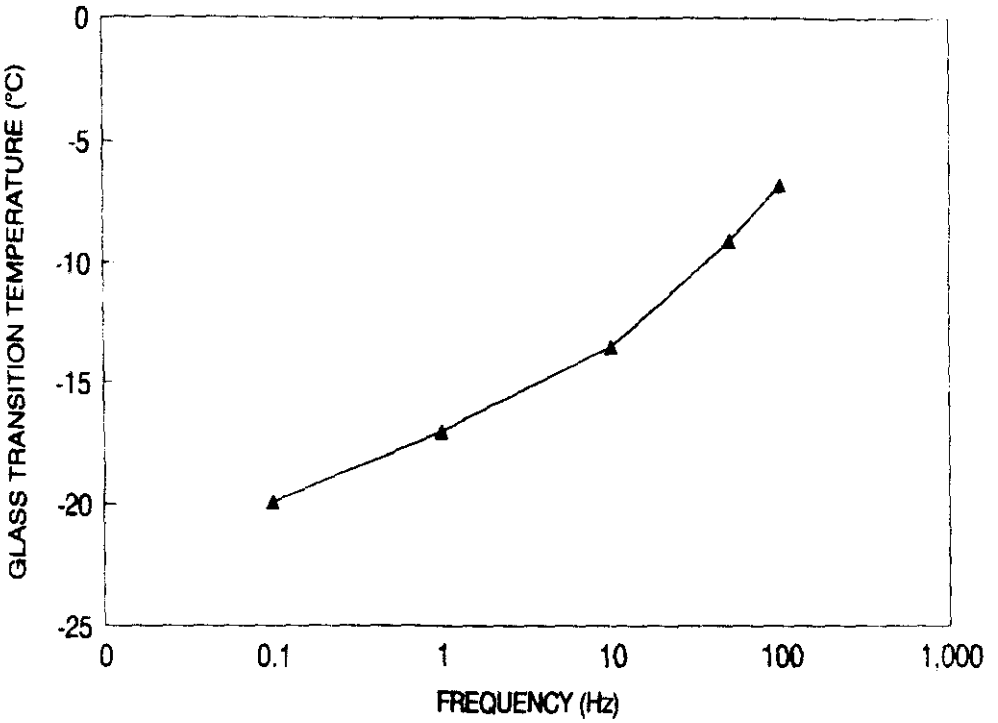

Figure 6.11. The effect of frequency on the glass transition temperature of $N_{50}P$

Table 6.4. Effect of blend composition and frequency on the tan δ_{max} values

Frequency (Hz)	Blend composition				
	N_0P	$N_{30}P$	$N_{50}P$	$N_{70}P$	$N_{100}P$
0.1	0.21	0.36	0.47	0.93	1.35
1.0	0.22	0.37	0.52	0.94	1.40
10.0	0.24	0.40	0.56	0.95	1.47
50.0	0.24	0.42	0.58	0.96	1.55
100.0	0.25	0.44	0.59	0.97	1.58

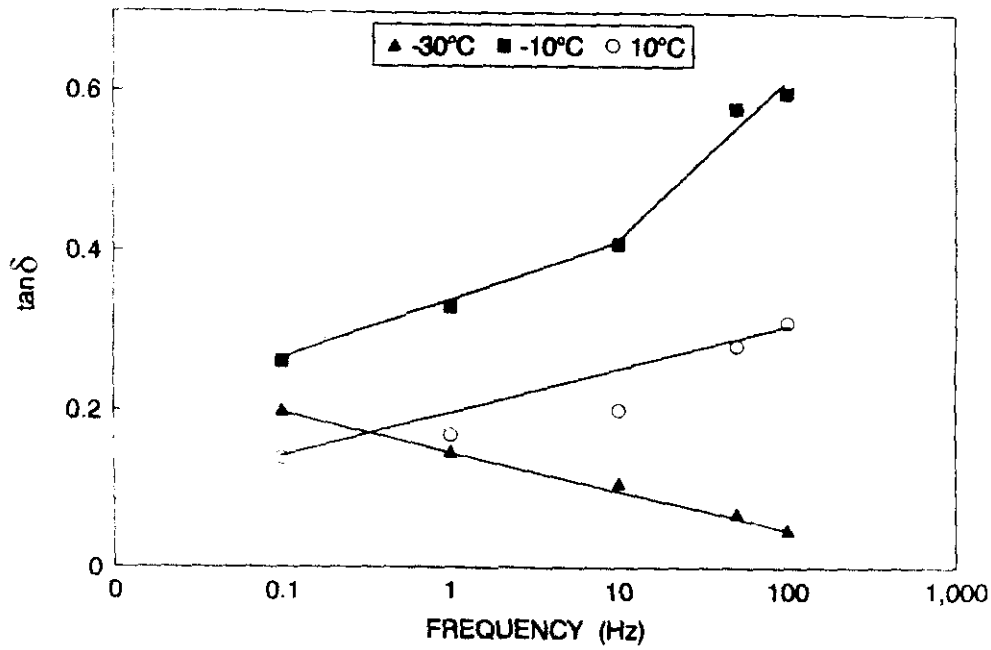

Figure 6.12. The variation in tan δ values of $N_{50}P$ as a function of frequency

The activation energy, E for the glass transition of the blends can be calculated from the Arrhenius relationship.

$$X = X_0 \exp(-E_x/RT) \qquad (6.1)$$

where X is the experimental frequency; X_0, a constant; E_x, the activation energy; R, the universal gas constant; and T, the absolute temperature. Activation energy is given in Table 6.5. The activation energy decreases with the increase in NBR content. This can be related to the amorphous nature of NBR. The flexibility increases with the NBR content. As the flexibility increases the activation process becomes easier and the activation energy decreases.

Table 6.5. Arrhenius activation energy for T_g of peroxide cured NBR/EVA blends

Sample code	ΔE (kJ/mol)
N_0P	605
$N_{30}P$	570
$N_{50}P$	504
$N_{70}P$	206
$N_{100}P$	37

The storage modulus (E′) versus temperature plots of $N_{50}P$ at different frequencies are shown in Figure 6.13. Here also the three distinct regions for the glassy, transition and rubbery regions are evident. In the glassy region all the blends exhibit similar moduli at all frequencies. In the transition and rubbery regions there is a marginal increase in modulus with increasing frequency. This variation is presented clearly in Figure 6.14 by plotting storage modulus of $N_{50}P$ at different temperatures against frequency. The variation in loss modulus (E″) with temperature of $N_{50}P$ at different frequencies are shown in Figure 6.15. In the glassy region (below T_g), the modulus decreases with increasing frequency. But in the rubbery region (above T_g), the trend is reversed, i.e., the modulus increases with increasing frequency. Interestingly, all the curves intersect at the transition region. The effect of frequency on the loss modulus of $N_{50}P$ at -30, -10 and 10°C is given in Figure 6.16. At -30°C, the modulus decreases marginally with frequency. But at -10 and 10°C, the modulus values increase with frequency.

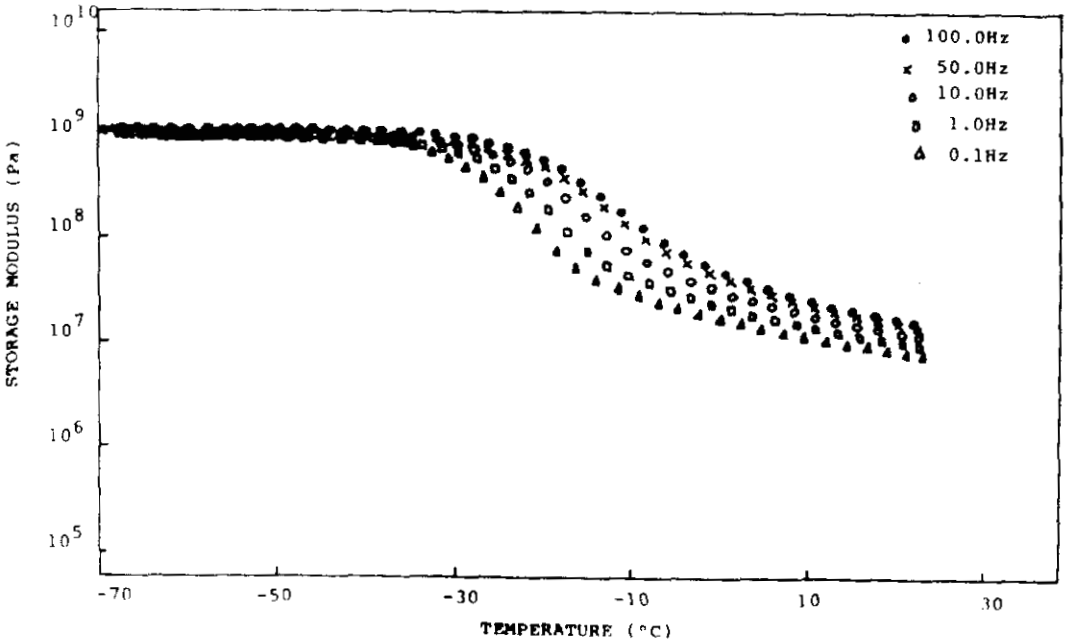

Figure 6.13. The variation in storage modulus of $N_{50}P$ with temperature

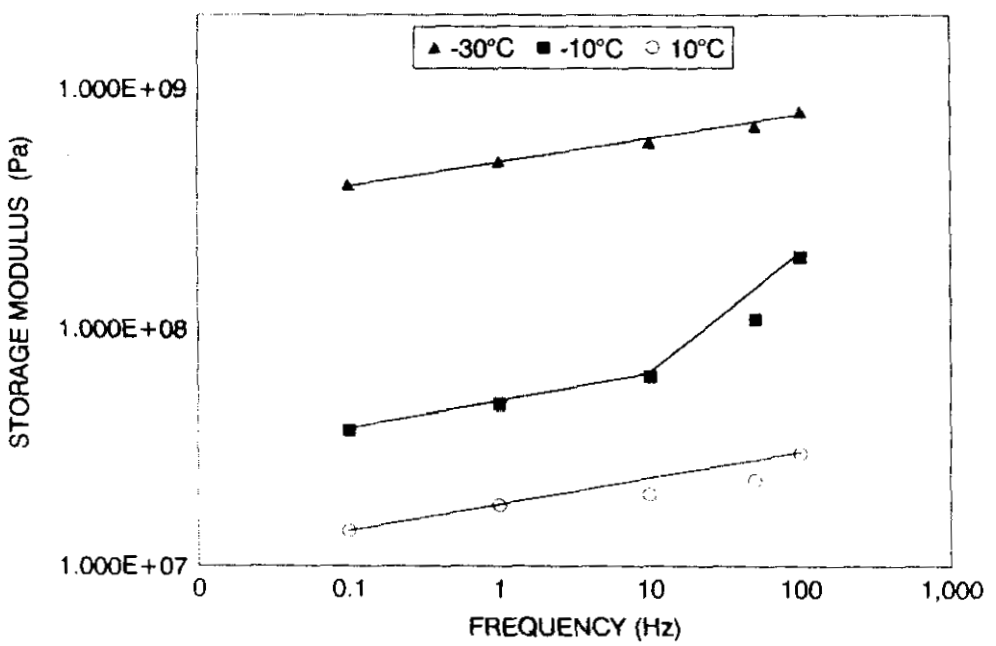

Figure 6.14. The variation in storage modulus of $N_{50}P$ with frequency

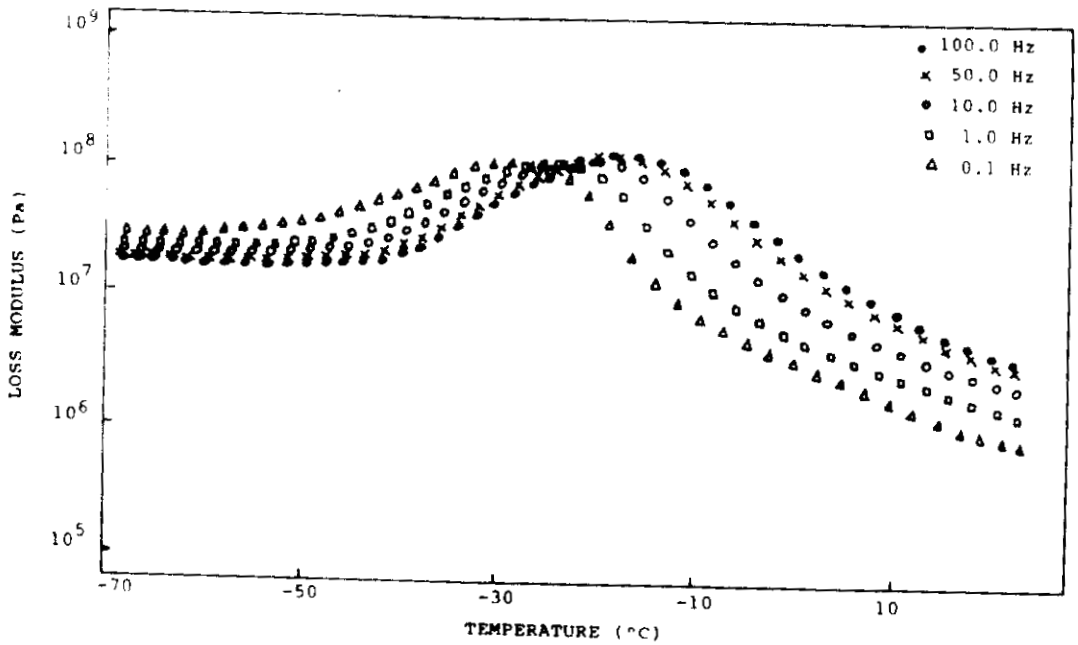

Figure 6.15. The variation in loss modulus of $N_{50}P$ with temperature

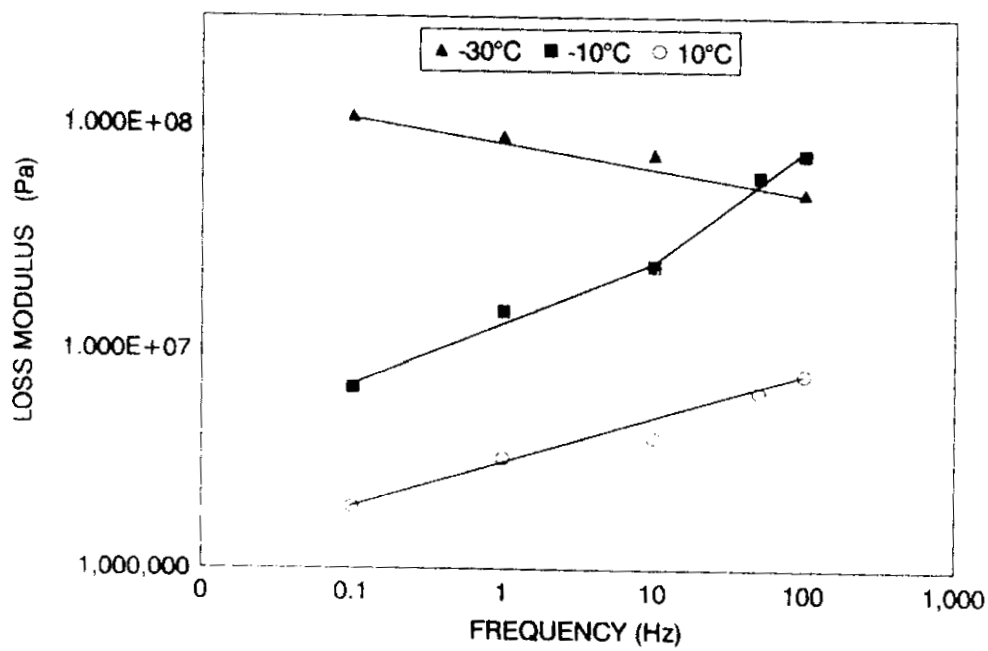

Figure 6.16. The variation in loss modulus of $N_{50}P$ with frequency

6.1.3 *Effect of crosslinking systems*

Figure 6.17 shows the dependence of loss tangent (tan δ) on temperature for uncrosslinked and various crosslinked systems of N_{50} at 50 Hz. The values of tan δ_{max}, T_g and crosslink density (ν) for uncrosslinked and various crosslinked systems of N_{50} at 50 Hz are given in Table 6.6. It is seen that the T_g shifts to a high temperature with crosslink density. The crosslink density of the samples is determined by swelling method as explained in Section 2.3.7(b). The effect of crosslink density on the T_g is also depicted in Figure 6.18. The tan δ_{max} values also exhibit the same trend as that of T_g (Table 6.6).

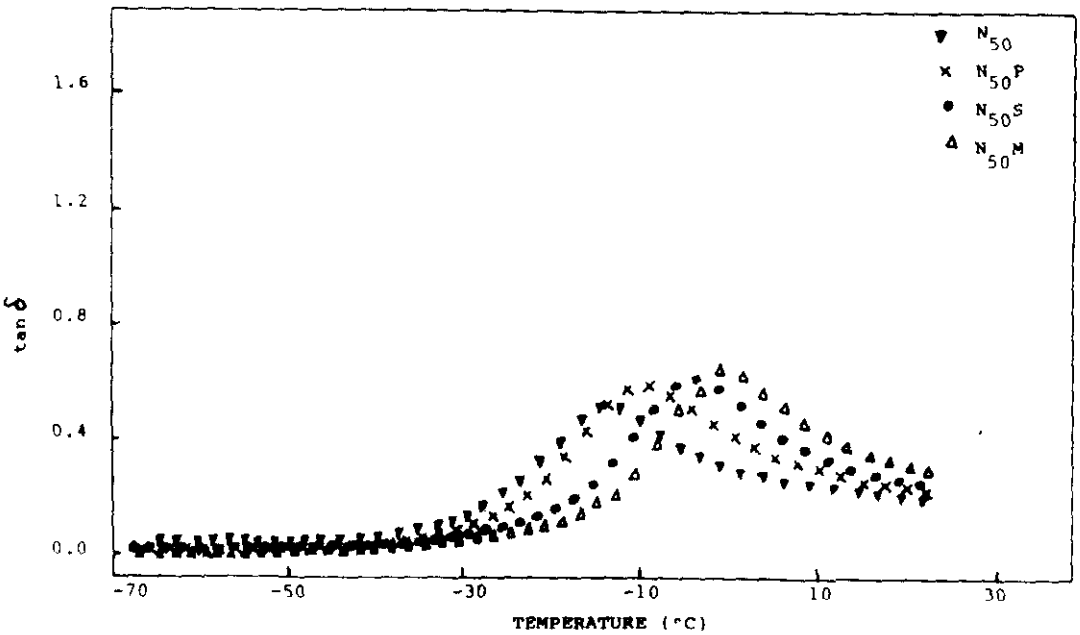

Figure 6.17. Influence of temperature on the tan δ values of various crosslinking systems of N_{50}

Table 6.6. Values of tan δ_{max}, T_g and ν for uncrosslinked and various crosslinking systems of N_{50} at 50 Hz

Samples	tan δ_{max}	T_g (°C)	$\nu \times 10^4$ gmol/cc
N_{50}	0.49	-12	-
$N_{50}P$	0.58	-9	2.84
$N_{50}S$	0.60	-3	3.01
$N_{50}M$	0.63	-1	3.25

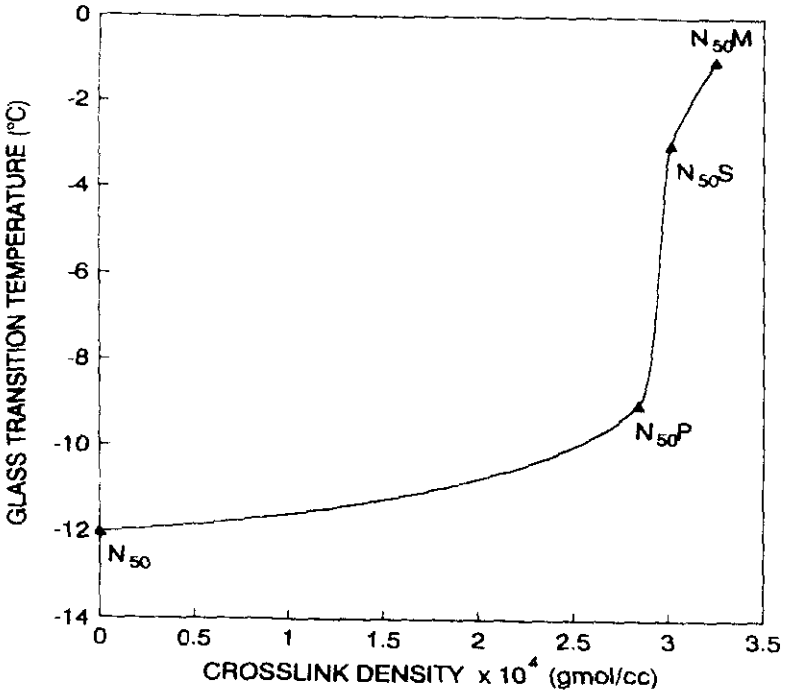

Figure 6.18. Effect of crosslink density on T_g

The dependence of temperature on the storage and loss moduli of different crosslinking systems is presented in Figure 6.19.

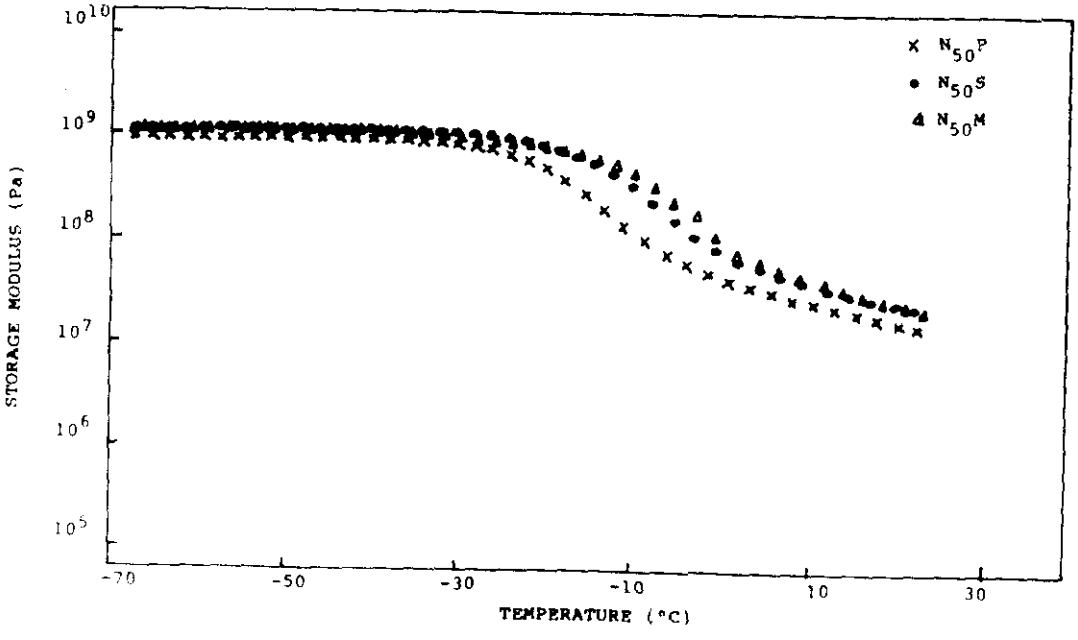

Figure 6.19. Influence of temperature on the storage modulus values for various crosslinking systems of N_{50}

The modulus values are low for the peroxide crosslinked system, which is having the lowest crosslink density. The three dimensional pictures giving the variations in tan δ with temperature and frequency of $N_{50}P$, $N_{50}S$ and $N_{50}M$ are represented in Figures 6.20-6.22. The peaks indicate the glass transition temperature of the blend. As the frequency increases the T_g is shifted to higher temperatures.

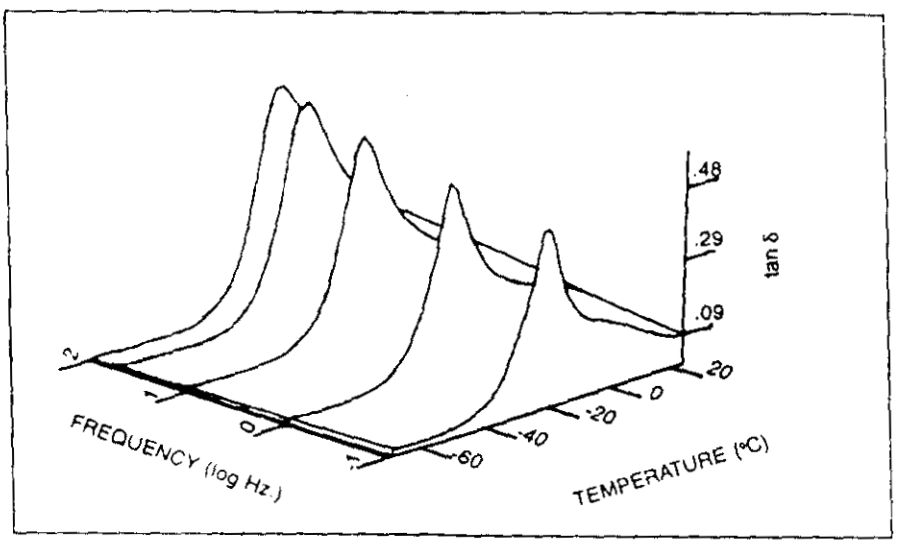

Figure 6.20. The variation in tan δ values of $N_{50}P$ with temperature and frequency

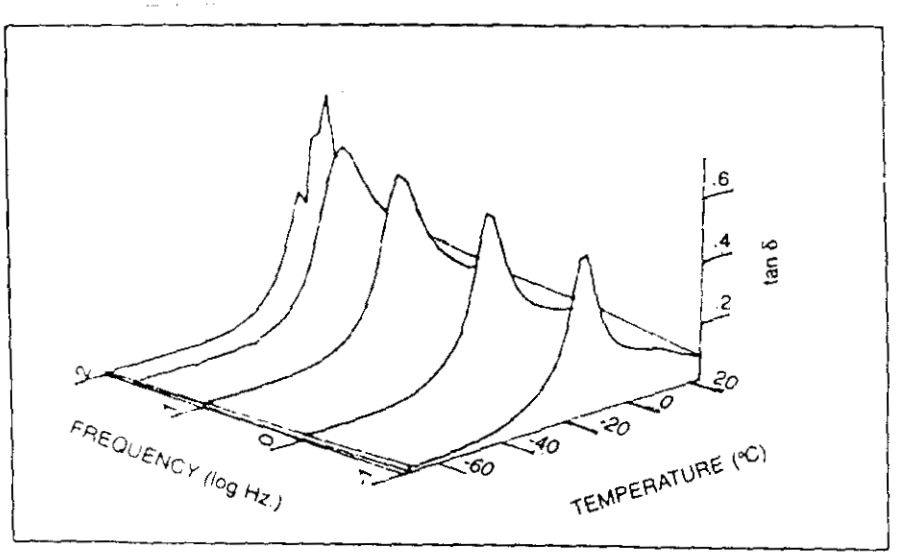

Figure 6.21. The variation in tan δ values of $N_{50}S$ with temperature and frequency

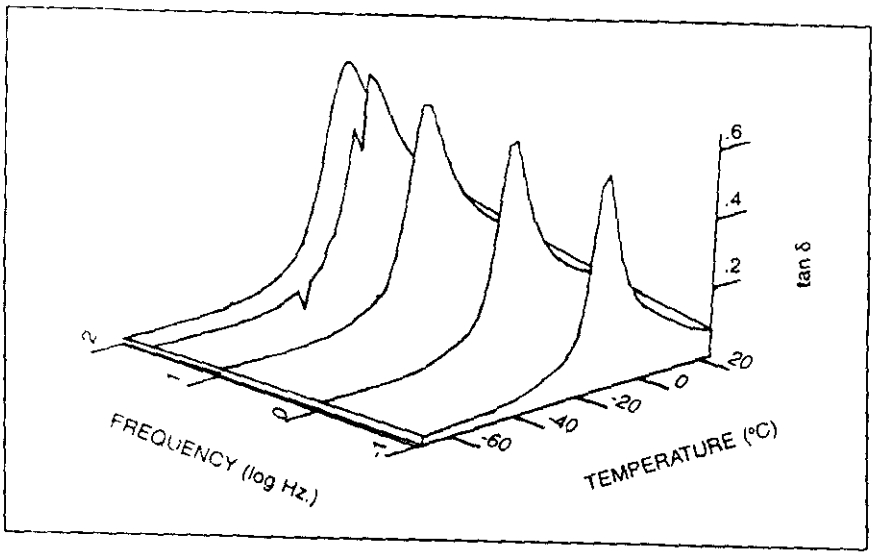

Figure 6.22. The variation in tan δ values of $N_{50}M$ with temperature and frequency

6.1.4 *Model fitting*

Applicability of various composite models such as parallel, series, Halpin-Tsai, Coran's, Takayanagi, Kerner and Kunori is examined to predict the viscoelastic behaviour of the blends. Details of all the equations are given in Section 3.1.3.

Model fitting for the storage modulus of peroxide cured blends at 50 Hz and 10°C is presented in Figure 6.23 and it is found that the experimental values lie close to the Coran's model for a value of n = 2. This implies that the modulus of NBR/EVA blends lies between the parallel upper bound model (M_U) and the series lower bound model (M_L). The applicability of Kerner's model for modulus-temperature and loss tangent-temperature data of uncrosslinked NBR/EVA blends have been investigated in detail by Bandyopadhyay *et al.*[12]

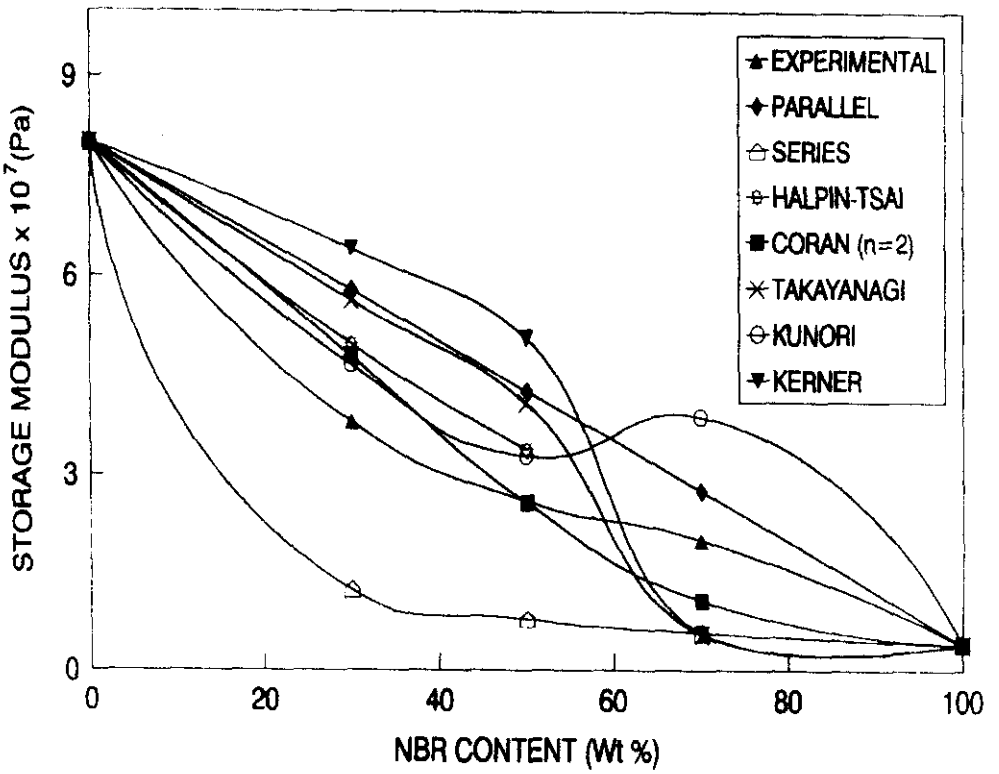

Figure 6.23. Applicability of various theoretical models to predict the storage modulus of NBR/EVA blends

6.1.5 Cole-Cole analysis

The Cole-Cole plots were drawn by plotting loss modulus (E″) against storage modulus (E′). Generally, homogeneous polymeric systems exhibit a semicircle diagram. Cole-Cole representation of miscible blends of poly(vinyl chloride) (PVC) and poly(α-methyl-α-n-propyl-β-propiolactone) (PMPPL) lead to the conclusion that this mixture does not exhibit micro-scale heterogeneities.[13] The Cole-Cole plots of $N_{30}P$, $N_{50}P$ and $N_{70}P$ are depicted in Figure 6.24. In all the blend compositions the values does not fall in a semicircle. This supports the heterogeneous nature of this blend.

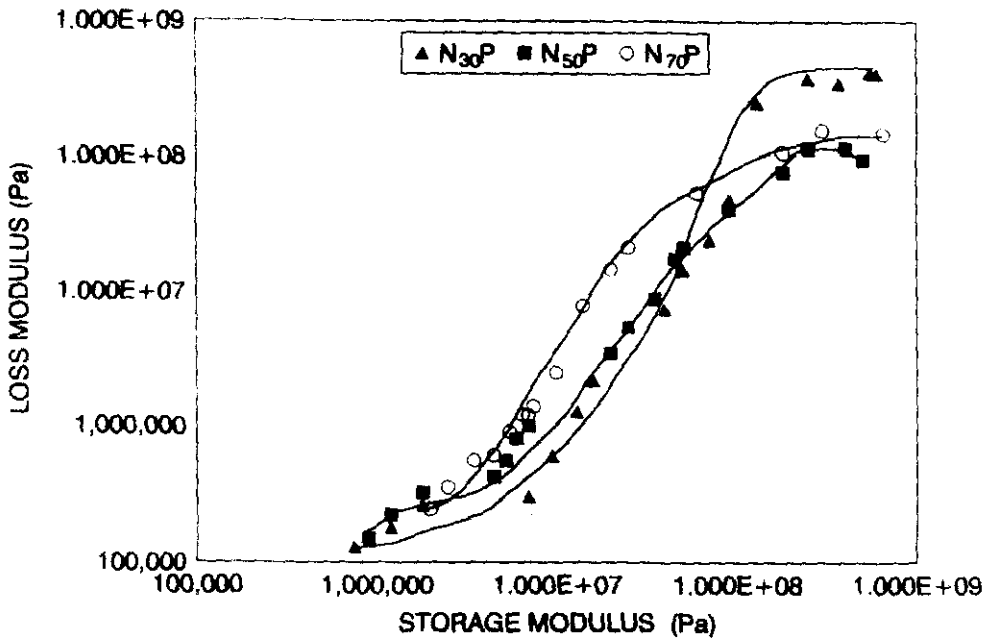

Figure 6.24. Cole-Cole plots of $N_{30}P$, $N_{50}P$ and $N_{70}P$

6.1.6 Time-temperature superposition analysis

Modulus of polymeric systems is a function of time as well as temperature. Due to the broad time dependence involved, it is not feasible to directly evaluate the complete behaviour of the modulus as a function of time at constant temperature. In principle, the complete modulus versus time behaviour of any polymer at any temperature can be measured. This is achieved by a shifting procedure that enables one to construct a 'master curve' which is based on the principle of time-temperature correspondence.[14,15] The master curve thus obtained is identical to that which could be measured at long times at a particular temperature.

The viscoelastic properties at a given frequency 'f' are quantitatively equivalent to those of an experiment carried out over a time $t = 1/2\pi f$. Viscoelastic data collected at one given temperature can be superimposed upon data collected at

different temperatures by shifting the curves, i.e., by using the time-temperature superposition principle. Figure 6.25 shows the log E' vs. log time graph for temperatures from -40 to 40°C.

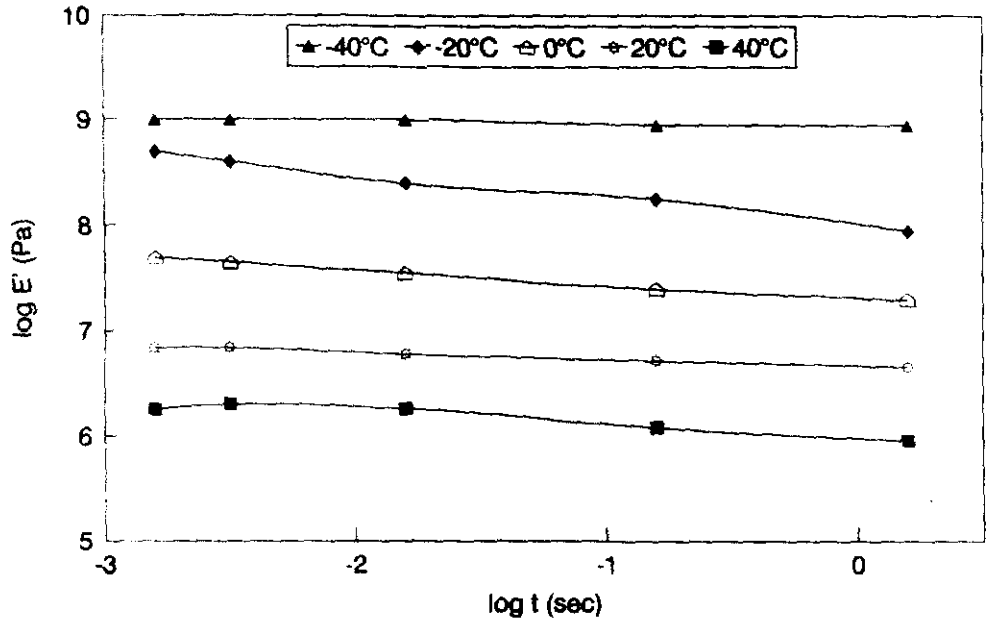

Figure 6.25. log E' vs. log t curves of NBR/EVA blends for temperatures from -40 to 40°C

Here the experimental curves of the modulus at different temperatures are plotted against log t. The modulus curve at a particular temperature is then shifted along the time axis until it overlaps with the next curve. The distance between curves gives the value of shift factor, log a_T. The shift factor characterises the rate of the relaxation mechanism at a particular temperature T_i in comparison with the rate at a higher temperature T_{i-1}. In this way log a_T values for all temperatures were determined. The master curve was constructed by plotting $\log(t/a_T)$ vs. log ET_0/T, where E is the storage modulus at a particular temperature, T_0 is the reference temperature on the Kelvin scale and T is the temperature of the

experiment. The temperature of 0°C was taken as the reference temperature in constructing the master curve. Figure 6.26 shows the master curve for $N_{50}P$.

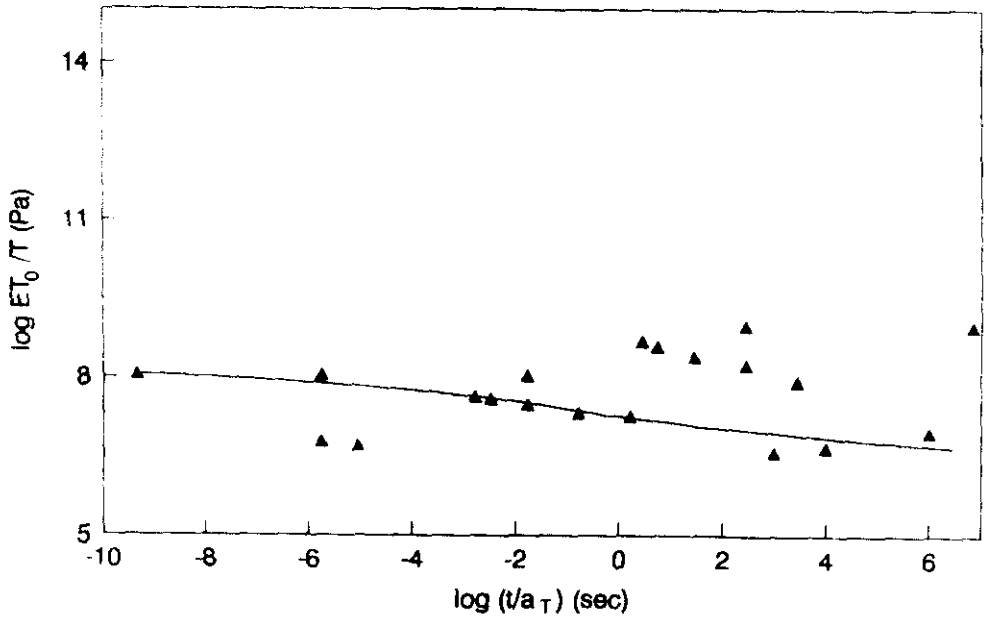

Figure 6.27. Plot of $\log(t/a_T)$ vs. $\log ET_0/T$

The main advantage of the master curve is that it provides modulus of the blend over a wide range of reduced time.

6.2 References

1. T. Murayama, *Dynamic Mechanical Analysis of Polymeric Materials*, John Wiley, New York, 1978.
2. B. E. Read and G. D. Dean, *The Determination of Dynamic Properties of Polymers and Composites*, Adam Hilger Ltd., Bristol, 1978.
3. M. J. Guest and J. H. Daly, *Eur. Polym. J.*, **26**, 603 (1990).
4. P. Ramesh and S. K. De, *J. Appl. Polym. Sci.*, **50**, 1369 (1993).
5. K. T. Varughese, G. B. Nando, P. P. De and S. K. De, *J. Mater. Sci.*, **23**, 3894 (1988).
6. M. Patri, A. B. Samui and P. C. Deb, *J. Appl. Polym. Sci.*, **48**, 1709 (1993).

7 Carmen del Rio and J. L. Acosta, *Polym. International*, **30**, 47 (1993).

8 R. E. Cohen and A. R. Ramos, *J. Macromol. Sci. Phys.*, **B17(4)**, 625 (1980).

9 J. W. Cho, S. Tasaka and S. Miyata, *Polym. J.*, **25**, 1267 (1993).

10 Y. Li and H. L. Williams, *J. Appl. Polym. Sci.*, **40**, 1891 (1990).

11 A. T. Koshy, B. Kuriakose, S. Thomas and S. Varughese, *Polymer*, **34**, 3428 (1993).

12 G. G. Bandyopadhyay, S. S. Bhagawan, K. N. Ninan and S. Thomas, *Rubber Chem. Technol.*, **70(4)**, 650 (1997).

13 T. M. Malik and R. E. Prud'homme, *Polym. Eng. Sci.*, **24**, 144 (1984).

14 J. J. Aklonis and W. J. MacKnight, *Introduction to Viscoelasticity*, John Wiley and Sons, 1983.

15 J. D. Ferry, *Viscoelastic Properties of Polymers*, 3rd Edn., Wiley, New York, 1980